



UNIVERSITAT
POLITÈCNICA
DE VALÈNCIA



UNIVERSITAT POLITÈCNICA DE VALÈNCIA

Escuela Técnica Superior de Ingeniería del Diseño

Implementación de un algoritmo para la optimización de trayectorias utilizando motores de bajo empuje

Trabajo Fin de Máster


Máster Universitario en Ingeniería Aeronáutica

AUTOR/A: Talave Campillo, Noel Raúl

Tutor/a: Morano Fernández, José Antonio

Cotutor/a externo: ACEDO RODRIGUEZ, LUIS

CURSO ACADÉMICO: 2022/2023



Algorithm implementation for trajectory optimization using low thrust motors



Master in Aeronautical Engineering



Master thesis

Author:

Talave Campillo, Noel Raúl

Tutors:

Moraño Fernández, José Antonio

Acedo Rodríguez, Luis

Julio 2023



UNIVERSITAT
POLITÀCNICA
DE VALÈNCIA

Algorithm implementation for trajectory optimization using low thrust motors

Author

Talave Campillo, Noel Raúl

Tutors

Moraño Fernández, José Antonio

Acedo Rodríguez, Luis



Master in Aeronautical Engineering



UNIVERSITAT
POLITÈCNICA
DE VALÈNCIA

Valencia, Julio 2023

Abstract

A crucial step in the development of space missions is the design of the trajectory that the spacecraft must follow. A simple definition of the objective of these trajectories is to reach from one point to another point in space fulfilling a series of requirements that can be of different types, such as the time of flight or fuel consumption, among others.

Spacecraft propelled by low-thrust engines are characterized by having thrust ranges around 1 N or even below that value, but they usually have a high specific impulse (1000 to 8000 s), making maneuvers with these engines very different from those performed with chemical engines, which, due to their greater thrust, are considered and therefore simulated as impulsive maneuvers. The high specific impulse allows carrying out missions similar to those of high thrust, reducing fuel consumption, and therefore favoring a greater payload, but the calculation of each trajectory requires a meticulous optimization study.

The main objective of this work is to implement a method for the optimization of trajectories between two celestial bodies using low-thrust engines. Optimization refers to the minimization or maximization of one or more objective variables, such as the time of flight t_f or consumed fuel mass. The final result shows that a low-thrust engine could minimize fuel consumption compared with impulsive trajectories. This result must be corroborated with the data of the Mars Orbiter Mission.

Key words

Trajectory optimization, Low-thrust.

Resumen

Una etapa esencial en el desarrollo de misiones espaciales es el diseño de la trayectoria que la nave debe seguir. Una definición simple del objetivo de estas trayectorias es la de llegar de un punto a otro punto del espacio cumpliendo una serie de requerimientos que pueden ser de diferentes tipos, como por ejemplo de tiempo de vuelo o de carga de combustible entre otros.

Las naves espaciales propulsadas por motores de bajo empuje se caracterizan por tener rangos de empuje en torno a 1 N o incluso por debajo de ese valor pero suelen tener un alto impulso específico (1000 a 8000 s), siendo las maniobras con estos motores muy diferentes a las realizadas con motores químicos, que al disponer de mayor empuje son consideradas y por tanto simuladas como maniobras impulsivas. El elevado impulso específico permite llevar a cabo misiones similares a las de alto empuje reduciendo el gasto de combustible, y por tanto, favoreciendo a una mayor carga de pago pero el cálculo de cada trayectoria requiere de un minucioso estudio de optimización.

El objetivo principal de este trabajo es implementar un método para la optimización de trayectorias entre dos cuerpos celestes utilizando motores de bajo empuje. La optimización hace referencia a la minimización o maximización de una o varias variables objetivo como por ejemplo el tiempo de vuelo t_f o la masa de combustible consumida. El resultado final muestra que un motor de bajo empuje podría minimizar el consumo de combustible en comparación con las trayectorias impulsivas. Este resultado debe ser corroborado con los datos de la Mars Orbiter Mission.

Palabras clave

Optimización trayectorias, Bajo empuje

Resum

Una etapa essencial en el desenvolupament de missions espacials és el disseny de la trajectòria que la nau espacial ha de seguir. Una definició senzilla de l'objectiu d'aquestes trajectòries és la d'arribar d'un punt a un altre punt de l'espai complint una sèrie de requisits que poden ser de diferents tipus, com ara el temps de vol o la càrrega de combustible, entre d'altres.

Les naus espacials propulsades per motors de baixa empenta es caracteritzen per tenir rangs d'empenta al voltant d'1 N o fins i tot per sota d'aquest valor, però solen tenir un alt impuls específic (1000 a 8000 s), sent les maniobres amb aquests motors molt diferents a les realitzades amb motors químics, que, en disposar de major empenta, són considerades i per tant simulades com maniobres impulsives. L'alt impuls específic permet dur a terme missions similars a les de baixa empenta reduint el consum de combustible, i per tant, afavorint una major càrrega útil, però el càlcul de cada trajectòria requereix d'un minuciós estudi d'optimització.

L'objectiu principal d'aquest treball és implementar un mètode per a l'optimització de trajectòries entre dos cossos celestes utilitzant motors de baixa empenta. L'optimització fa referència a la minimització o maximització d'una o diverses variables objectiu, com ara el temps de vol t_f o la massa de combustible consumida. El resultat final mostra que un motor de baixa empenta podria minimitzar el consum de combustible en comparació amb les trajectòries impulsives. Aquest resultat ha de ser corroborat amb l'obtenció de les dades completes de la Mars Orbiter Mission.

Paraules clau

Optimització de trajectòries, baixa empenta.

Acknowledgements

Gracias a ti, Ñoño.

*Por lo que quizás seré, niego el mundo como es.
Sin brindar, celebraré los días no vividos.*

Santi Balmes

Contents

I	Report	2
1	Introduction	3
1.1	Motivation and goal	3
2	State of the art	5
2.1	Trajectory Optimization Research	5
2.2	Space missions	7
3	Theoretical background	9
3.1	Orbital mechanics	9
3.1.1	Coordinate systems	9
3.1.2	Two-body problem - Equation of motion	12
3.1.3	Impulsive and non-impulsive maneuvers	14
3.1.4	Interplanetary Trajectories	15
3.2	Spacecraft trajectory optimization	16
3.2.1	Approaches	16
3.2.2	Particle Swarm Optimization	18
3.2.3	Sequential Quadratic Programming	20
4	Methodology	23
4.1	Fuel-optimal problem with Homotopic approach	23
4.1.1	Introducing the dynamic and conditions of the system	23
4.1.2	Calculating the optimal control	24
4.1.3	The homotopic approach	27
4.2	Time-optimal problem	27
4.3	Algorithm structure	28
5	Results	33
5.1	PSO Validation	33
5.2	Hybrid algorithm validation	35
5.3	Real mission comparison	39
6	Conclusions and future studies	43

II	Budget and specifications	47
7	Specifications	49
7.1	Introduction	49
7.2	Appendix I: General safety conditions in workplaces	49
7.3	Order, cleaning and maintenance	50
7.4	Appendix III: Environmental conditions of workplaces	51
7.5	Appendix IV: Lighting of workplaces	51
7.6	Appendix V: Toilet facilities and rest areas	51
7.7	Appendix VI: First aid materials and facilities	51
8	Budget	53
8.1	Introduction	53
8.2	Cost breakdown	53
8.2.1	Material	53
8.2.2	Personnel hours	55
8.2.3	Electricity consumption	55
8.3	Final cost	56
8.4	Commercial profit	56

List of Figures

2.1	Overview of investigated Low-Thrust Optimization tools David Morante (2021)	6
2.2	Deep Space 1 badge Wikipedia (2023a)	7
2.3	DART spacecraft NASA (2023a)	8
3.1	SCI and ECI coordinate systems Koks (2017)	11
3.2	SCI coordinate system Koks (2017)	11
3.3	Two point masses located in an inertial reference frame Weber (2023) .	12
3.4	Interplanetary trajectory Weber (2023)	15
3.5	Pros and cons of optimization approaches David Morante (2021)	18
3.6	Possible objective function definition Abolfazl Shirazi (2018)	19
4.1	Flowchart for the Fuel-optimal problem	29
5.1	PSO validation - Objective function vs Iteration	35
5.2	PSO validation - Costates vs Time	35
5.3	Hybrid algorithm validation - Objective function vs Iteration	37
5.4	Hybrid algorithm validation - Costates vs Time	37
5.5	Hybrid algorithm validation - Thrust and Mass vs Time	38
5.6	Hybrid algorithm validation - Orbital trajectory	38
5.7	Real mission comparison - Thrust and Mass vs Time	40
5.8	Real mission comparison - Orbital trajectory	41

List of Tables

5.1	PSO validation	34
5.2	Hybrid algorithm validation	36
5.3	Hybrid algorithm validation - Error rendezvous	36
5.4	Real mission comparation	39
5.5	Real mission comparation - Error rendezvous	40
8.1	Annual depreciation cost	54
8.2	Computer license total cost	54
8.3	Cost of writing materials	54
8.4	Personnel hours cost	55
8.5	Electricity consumption	55
8.6	Final cost	56

Part I

Report

Chapter 1

Introduction

1.1 Motivation and goal

When economic, political, or social circumstances cause the appearance of necessities in relation to space applications, the design of space missions is undoubtedly of major importance. During this process, several space engineering disciplines are involved and must coexist within one idea, to accomplish the mission objectives.

The orbit design takes an essential role in the mission analysis field, as it could largely limit and define part of the requirements for the rest of the subsystems of the spacecraft. For instance, the orbit definition influences the time of flight, the spacecraft's mass, and the proper mass distribution in the spacecraft.

On the one hand, it is clear how the spacecraft's trajectory could impact the time of flight. On the other hand, the mass-related objectives could be sometimes non-clear. First, the propellant mass is directly dependent on the orbit definition. Normally, the fuel consumption is associated with the time of flight. The more the flight of time, the more the expended mass. Nonetheless, this idea gets complicated when gravitational assistances and engine power cut appears.

Regarding this mass problem, the fuel mass of the spacecraft modifies the payload mass, which might affect the accomplishment of the mission. Having the change of improving the payload capacity (more scientific instruments or even more humans to a Mars mission) could affect significantly the development of society from an economic point of view.

For this reason, the optimization of spacecraft trajectories focusing on continuous low-thrust models is of big relevance for its potential improvements in reducing the fuel consumption of a spacecraft. Hence, the current master thesis pretends to contribute to this field's enhancement by developing an algorithm that minimizes the fuel consumption of a spacecraft trajectory.

Chapter 2

State of the art

This chapter provides the current knowledge about Low-thrust Trajectory Optimization. First, a search on trajectory optimization is performed where different articles are presented. Finally, it is shown some of the real missions who has been using this technology.

2.1 Trajectory Optimization Research

It has been found several articles that focus on spacecraft trajectory optimization. First, there exist two big brunches depending on the thrust model: Impulsive thrust or Continuous low-thrust.

Impulsive trajectories have been the first type of thrust model used since the beginning of the aerospace era (see Section 3.1.3). One of the main reasons is its trajectory design simplicity compared with continuous thrust, where the approach to compute its trajectories are normally numerical (see Section 3.2).

On the one hand, impulsive trajectories have been used for several missions such as interplanetary rendezvous in Bastida Pertegaz (2021) or Fernando Alonso Zotes (2011), where the impulse Δv is obtained by gravitational assistant. These types of trajectories are also implemented with numerous multi-impulses that try to replicate the continuous behavior of continuous low-thrust engines. For instance, in Ya-Zhong Luo (2006) it is presented a multiple-impulsive model with the goal of minimizing the time of flight t_f for rendezvous missions. Finally, in Jiang Xiao-yong (2013) it is fully validated the availability and efficiency of the Multi-Impulsive Extended method for Low-Thrust Trajectory Optimization.

On the other hand, in spite of its complexity to simulate and design, continuous thrust trajectories have been also studied due to its possible improvement on the time of flight t_f and fuel consumption Δm when deep space missions are considered. For

instance, Anne Schattel (2016) uses a low-thrust continuous model for an autonomous asteroid rendezvous mission. In the end, it is found that a low-thrust model reduces the fuel mass and raises the capabilities for long-term space missions.

The thrust model is not the only important aspect of trajectory optimization, there are also several mathematical approaches to get the optimal value of the problem. Considering a numerical approach, the solutions can be divided depending on if a Deterministic (Gradient-based), Heuristic, or Hybrid method has been used (see subsection 3.2.1).

The Sequential Quadratic Programming (SQP) is one of the typical deterministic approaches used in this kind of application as presented in Betts (2000) or Parrish & Scheeres (2016). However, there are other approaches as the interior point method used in Frederiksen (2021). Considering the heuristic methods, the most famous ones are the population based-algorithms where Particle Swarm Optimization (PSO) and Genetic Algorithms (GA) are deeply used. Abolfazl Shirazi (2018) shows several articles where PSO and GA algorithms are applied. In total, for continuous thrust models, there are around 19 studies using GA and 11 references for the PSO. Finally, hybrid methods use both, deterministic and heuristic algorithms. For example, Jiang (2012) uses a PSO to initialize the algorithm and then applies the software MinPack-1 (very similar to the `fsolve` function implemented in MATLAB).

Finally, Figure 2.1 can be seen as a general comparison between the different approaches used in commercial and research tools for continuous low-thrust trajectory optimization.

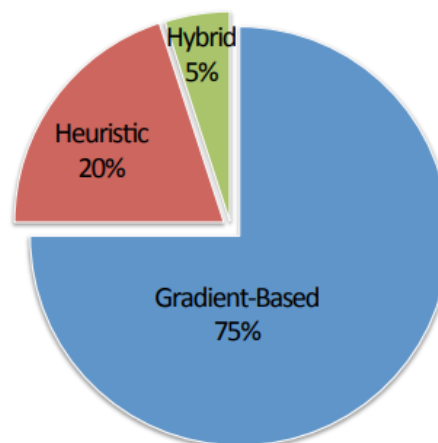


Figure 2.1: Overview of investigated Low-Thrust Optimization tools David Morante (2021)

2.2 Space missions

In this section, it is enumerated and briefly explained several spacecrafts that used low-thrust models during some part of their mission.

The first demonstration of a low-thrust thruster was the NASA SERT-1 spacecraft using an ion thruster. It was launched in 1964 and operated for 31 minutes (Wikipedia (2023g)). However, one of the most renowned missions carried out by NASA was Deep Space 1 in 1998. The goal of this mission was simply to be a technology demonstrator. It also orbited one asteroid and one comet. The spacecraft had implemented an Xenon ionic engine called NSTAR with a maximum thrust value of 0.09 Newtons (Wikipedia (2023a)). The mission badge can be seen in Figure 2.2.



Figure 2.2: Deep Space 1 badge Wikipedia (2023a)

Furthermore, other space agencies around the world have performed low-thrust missions such as the Japan Aerospace Exploration Agency (JAXA) with the Hayabusa spacecraft in 2003 (Wikipedia (2023c)). Nevertheless, one of the most recent space missions successfully performed was the Double Asteroid Redirection Test (DART) mission by NASA. The purpose was to assess how much a spacecraft's impact deflects an asteroid orbit. It finally impacted on September 26th, 2022 (Wikipedia (2023b)).

The spacecraft, shown in Figure 2.3, had installed the NEXT-C thruster. This is a Xenon thruster with a maximum thrust of 0.237 Newtons and a specific impulse of 4190 seconds (W. Andrew Hoskings & M. Monheiser (2007)). In fact, this is the thruster model that is used for the space mission application in Chapter 5 between the Earth and Mars. Nevertheless, in this case, it is used two NEXT-C engines to increase the thrust value up to 0.47 Newtons.

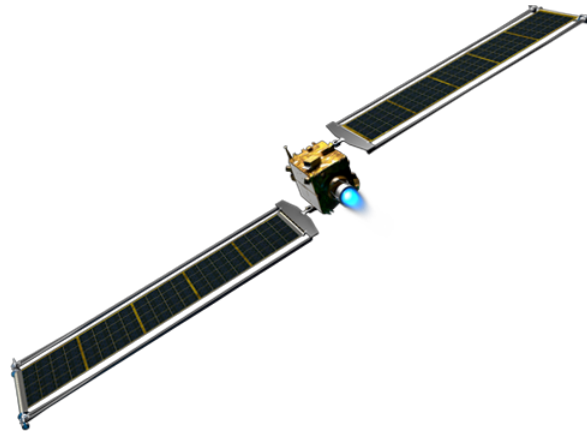


Figure 2.3: DART spacecraft NASA (2023a)

After analyzing the results, NASA concluded that the DART spacecraft successfully collided with Dimorphos on 26 September 2022 at 23:14 UTC and shortened its orbit by 32 minutes (Wikipedia (2023b)).

Chapter 3

Theoretical background

The purpose of this chapter is to facilitate the reader with the theoretical background needed for the clear comprehension of the study. Therefore, it pretends to be a guideline where several concepts are explained.

First, pure Orbital Mechanics theory is presented. Here, the basic principles, equations, and expressions development are described in a logical order to increase the understanding of the problem.

Finally, it is illustrated specific spacecraft trajectory optimization notions. In fact, the idea is to show the different mathematical approaches in order to solve these problems but also to expose the logic behind the algorithms used for computing the problem.

3.1 Orbital mechanics

Orbital mechanics is a field that contains a large amount of information. For this reason, the section only presents the minimum information to make the methodology understandable. For further details, books such as Curtis (2020) and Hintz (2015) explain the ideas in depth.

3.1.1 Coordinate systems

The coordinate system represents the structure that allows to define clearly lines, points, or surfaces on a manifold such as the Euclidean space (Wikipedia (2022)).

For orbital mechanics, coordinates systems describe the position of objects such as planets, spacecraft, galaxies, etc. Depending on how these coordinates need to be presented, there exist different coordinate systems definitions.

For defining a coordinate system it is needed: The origin, the reference plane, and the principal direction. Based on this, for defining the orbital trajectories of a spacecraft within our solar system, are normally used the followings:

- Geocentric equatorial system
- Geocentric ecliptic system
- Heliocentric equatorial system
- Heliocentric ecliptic system

Geocentric represents a coordinate system where the origin is the Earth, and Heliocentric is when the origin is the Sun. At the same time, equatorial illustrates that the reference plane is the Earth's equator and ecliptic represents the imaginary plane that contains the Earth's orbit around the Sun.

There also exists the International Celestial Reference System (ICRS), the current standard celestial reference system adopted by the International Astronomical Union (IAU) (Wikipedia (2023d)). In this case, the origin is the barycenter of the solar system.

There is another critical point when a coordinate system needs to be fully defined. The system can or cannot be inertial. An inertial frame is a coordinate system that is not accelerated, meanwhile, the non-inertial frame is accelerated. An example of a non-inertial frame is the ECEF (Earth-centered, Earth-fixed). In this case, the coordinate system rotates with the Earth as the X axis follows the prime meridian (Greenwich meridian).

For this study, only inertial frames are used. To better understand this concept, it can be seen in Figure 3.1 how the SCI (Sun-centered inertial) and the ECI (Earth-centered inertial) are described.

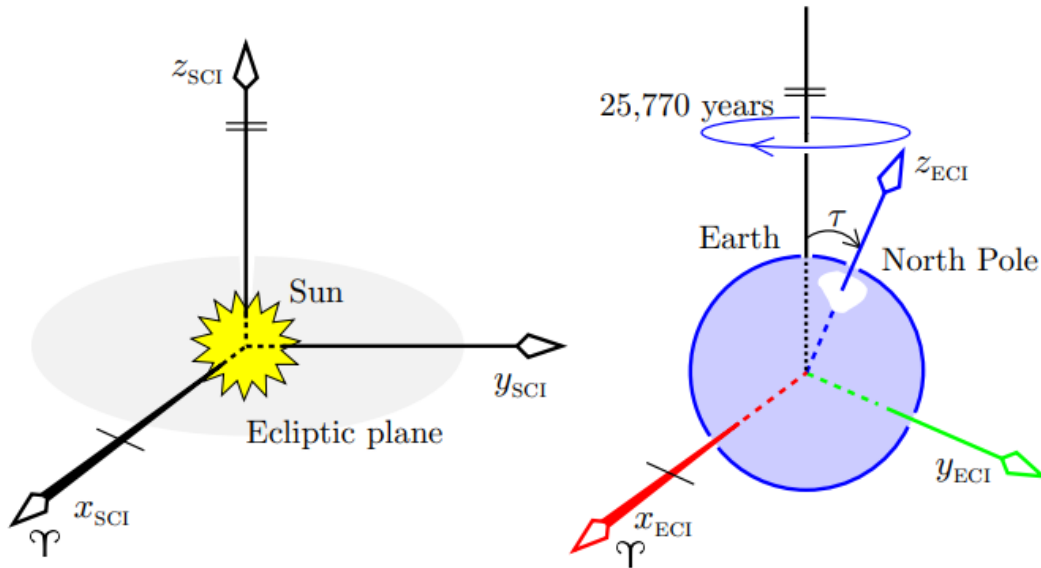


Figure 3.1: SCI and ECI coordinate systems Koks (2017)

The characteristic that makes these systems inertial is its x_{SCI} and x_{ECI} vector. This direction is pointing to the March Equinox, which occurs when the Sun crosses the equatorial plane from below (Weber (2023)). As Figure 3.2 indicates, the x_{SCI} points to this Equinox, also known as Aries Point.

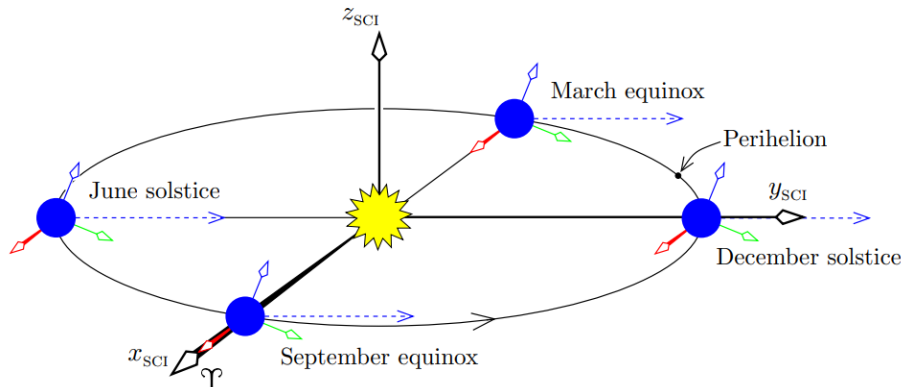


Figure 3.2: SCI coordinate system Koks (2017)

So, the use of these coordinate systems depends on the application. Normally, the ECI coordinate system is used for studying the movement of satellites around the Earth, meanwhile, the SCI coordinate system is for studying celestial bodies that orbit the Sun. Consequently, for this Master Thesis, the SCI coordinate system is applied due to its mission, an interplanetary rendezvous.

3.1.2 Two-body problem - Equation of motion

In order to know what is the relative motion of a spacecraft with the Sun, it is needed to obtain the differential equation that defines this motion. For this, Figure 3.3 illustrates a drawing of two point masses, m_1 and m_2 that is affected by the other's gravitational pull.

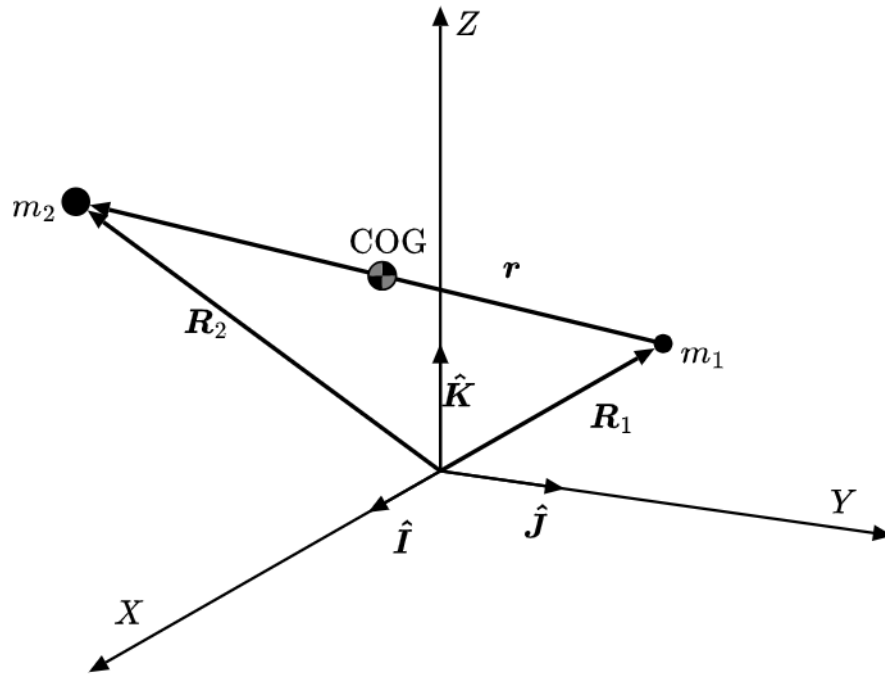


Figure 3.3: Two point masses located in an inertial reference frame Weber (2023)

This gravitational pull is described by considering Newton's law of gravitation. This law is linked with Newton's second and third laws as follows.

Newton's third law in Equation 3.1 presents the equality between these two body's forces.

$$\mathbf{F}_{12} = -\mathbf{F}_{21} \quad (3.1)$$

Nevertheless, thanks to Newton's second law, the forces \mathbf{F}_{21} and \mathbf{F}_{12} can be described as a function of each mass acceleration in Equation 3.2.

$$\begin{aligned} \mathbf{F}_{12} &= m_1 \ddot{\mathbf{R}}_1 \\ \mathbf{F}_{21} &= m_2 \ddot{\mathbf{R}}_2 \end{aligned} \quad (3.2)$$

Straightaway, the unique force acting on the system is the gravitational force. So, the values of these forces can also be described as Equation 3.3. G is called the gravitational constant.

$$\begin{aligned} F_{12} &= \frac{Gm_1m_2}{r^2}\mathbf{u}_r \\ F_{21} &= -\frac{Gm_1m_2}{r^2}\mathbf{u}_r \\ \mathbf{u}_r &= \frac{\mathbf{r}}{r} \end{aligned} \quad (3.3)$$

Finally, by combining Equation 3.2 and Equation 3.3, the mass acceleration can be described as a function of the distance between masses in Equation 3.4.

$$\begin{aligned} \ddot{\mathbf{R}}_1 &= \frac{Gm_2}{r^2} \frac{\mathbf{r}}{r^3} \\ \ddot{\mathbf{R}}_2 &= -\frac{Gm_1}{r^2} \frac{\mathbf{r}}{r^3} \end{aligned} \quad (3.4)$$

During the study, one of the masses (the Sun) is the origin of the inertial coordinate system. So, the idea is to get a differential equation that explains the time dependency with \mathbf{r} . For this, taking into account Equation 3.5 and Equation 3.4, Equation 3.6 is obtained.

$$\ddot{\mathbf{r}} = \ddot{\mathbf{R}}_2 - \ddot{\mathbf{R}}_1 \quad (3.5)$$

The final expression only considers the mass m_1 as it is simplified assuming that $m_1 \gg m_2$. In this case, m_1 is the Sun's mass and m_2 is the spacecraft's mass. μ is the standard gravitational parameter.

$$\begin{aligned} \ddot{\mathbf{r}} &= -G(m_1 + m_2) \frac{\mathbf{r}}{r^3} = -\mu \frac{\mathbf{r}}{r^3} \\ \mu &\approx Gm_1 \end{aligned} \quad (3.6)$$

It is important to mention that this is the Equation of Motion of an object orbiting one principal object, without considering any other gravitational pull from other celestial bodies. Equation 3.7 shows the general N-body problem equation of motion with other possible accelerations $\mathbf{\Gamma}$ other than the gravitational forces, such as the spacecraft's thrust, Earth's oblateness J2, aerodynamic forces, etc.

$$\ddot{\mathbf{r}} = -G \sum_{i=1}^N \frac{m_i(\mathbf{r} - \mathbf{r}_i)}{|\mathbf{r} - \mathbf{r}_i|^3} + \mathbf{\Gamma} \quad (3.7)$$

For this problem, the Equation of Motion is going to be defined by Equation 3.6 and adding an extra term for the spacecraft's thrust. Therefore, it is considered a two-body problem with thrust as the only perturbation.

3.1.3 Impulsive and non-impulsive maneuvers

In this subsection it is not explained the process of calculating orbital maneuvers as it is already well explained in books such as Curtis (2020) and Hintz (2015). The goal is to explain the differences between impulsive and non-impulsive maneuvers.

One of the key concepts, in order to understand this study, is to be familiarized with orbital maneuvers. The continuous low-thrust engines promote what is called non-impulsive maneuvers as these apply the force over a significant time. Nevertheless, there are also impulsive maneuvers where the force is only applied during a short period of time.

On the one hand, when an impulsive maneuver is required, the purpose is to perform a variation in the spacecraft's velocity Δv . This change of velocity has associated the consumption of the propellant mass as described in Equation 3.8. As can be observed, to calculate this Δm it is not needed any time information as it is assumed this maneuver happens in an infinitesimal interval of time.

$$\frac{\Delta m}{m} = 1 - e^{\frac{-\Delta v}{I_{sp}g_0}} \quad (3.8)$$

where Δm is the variation of propellant mass, m is the mass of the spacecraft, g_0 is the gravitational acceleration and I_{sp} the specific impulse. In turn, the specific impulse I_{sp} is the Thrust T per unit of mass flow rate of propellant expended.

On the other hand, a non-impulsive maneuver demands the integration of Equation 3.9 to calculate the variation of mass through the trajectory. Moreover, the velocity change is progressive and normally has lower values compared with impulsive maneuvers.

$$\dot{m} = -\frac{T}{g_0 I_{sp}} \quad (3.9)$$

As shown in these two equations, the higher the I_{sp} , the less fuel consumption of

the spacecraft. In fact, this is the reason why low-thrust engines could improve the reduction of mass due to their high values of specific impulse compared with impulsive engines.

3.1.4 Interplanetary Trajectories

When the mission is to perform an interplanetary trajectory, there could be different ways to obtain some results. One option is to directly apply the Equation 3.7 and consider all the possible perturbations, which will be generally the presence of other planets. Nevertheless, this is very computationally expensive. Another way is to apply what is called the Method of Patched Conics (Wikipedia (2023f)).

The idea of this method is to divide the whole interplanetary transfer into three different trajectories. The first path is called hyperbolic trajectory, and its main goal is to escape from the gravitational pull of the initial planet. The next part creates an elliptical trajectory to pass from the initial planet to the final planet. Finally, with another hyperbolic trajectory, it is possible to arrive to the final planet.

The sphere of influence is the imaginary sphere that represents the boundary where the planet's gravitational influence on the spacecraft is stronger than the Sun's (Weber (2023)). Therefore, its trajectory starts and ends once the spacecraft is inside or outside this sphere. This process can be observed in Figure 3.4

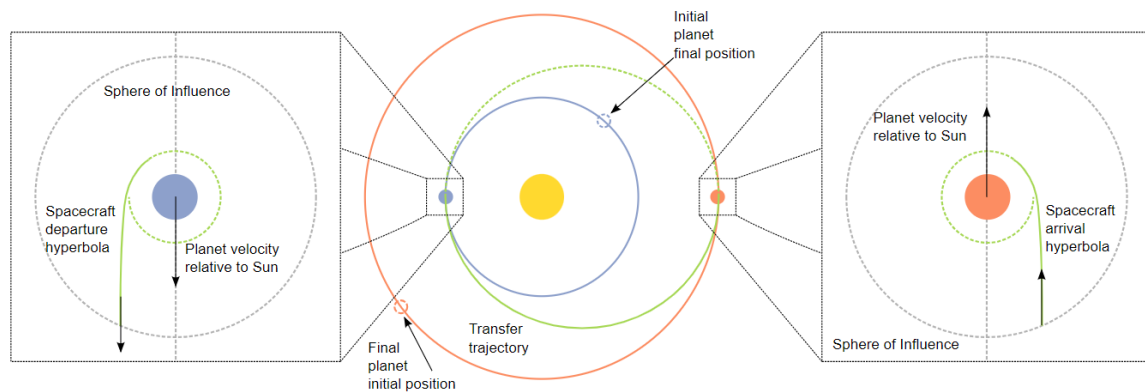


Figure 3.4: Interplanetary trajectory Weber (2023)

Nevertheless, for this Master Thesis, the trajectory is going to be integrated with no perturbation from other planets. Hence, the initial/final position and velocity of the spacecraft are going to be equal to the position and velocity vector of each initial and final planet.

3.2 Spacecraft trajectory optimization

This current section presents the different approaches to solving the problem of spacecraft trajectory optimization from a mathematical point of view. Finally, the last two sections describe the logic behind the two algorithms selected for computing the results.

3.2.1 Approaches

When optimizing a spacecraft trajectory there exists two types of approaches: analytical and numerical approaches.

On the one hand, analytical approaches represent an optimal trajectory with an analytical expression. Due to the usual complexity of this problem, these approaches are rarely for this kind of application. One example of an analytical solution could be the Hohmann transfer. This transfer can be seen in the center of Figure 3.4, where the analytical trajectory gives the optimal path for minimizing fuel consumption when impulsive engines are used (Abolfazl Shirazi (2018)).

On the other hand, numerical approaches are also considered in the investigations. Clearly, numerical approaches make use of some numerical computation in order to get the final solution. At the same time, the numerical approaches can be divided into two methods: Direct and indirect methods.

The direct method converts the optimal control problem into an optimization problem considering the discretization of the states and control vectors. Then, the system of differential equations is integrated. The final goal is to find the discrete representation of the state and the control of the trajectory that satisfy a set of nonlinear constraint equations and the equality and inequality restrictions (Abolfazl Shirazi (2018)). This method is easier to execute compared with the indirect methods, but they are less accurate. At the same time, a direct method has a larger radius of convergence but the optimality of the solution is not guaranteed Abolfazl Shirazi (2018).

The indirect methods use the same techniques as the direct methods with the difference of having analytic expressions and conditions that promote the optimality of the solution. It means that the purpose now is to guarantee that the parameters of these analytic expressions satisfy a series of optimality constraints. The analytic expressions are obtained by applying the Optimal Control Theory that relies on Pontryagin's Minimum Principle (PMP) (Abolfazl Shirazi (2018)). In this case, due to PMP, a series of Lagrange multipliers or costates vectors are integrated with the state vector of the system. Although the indirect methods are more accurate, their radius of convergence is smaller and they do not have the same flexibility as direct methods because of the derivation of the costate differential equations for each different problem.

These are the two main methods for solving numerically the problem. Furthermore,

there are different techniques to establish the dynamic of the system in the solution. First, the single shooting technique integrates the trajectory by unknowing the initial state of the costates, but knowing the initial and final value of the vector state. Secondly, the multiple shooting integrates over different subintervals of time $[t_i, t_{i+1}]$ where the initial value of the costates is unknown and needs to be determined (David Morante (2021)). Finally, the collocation technique discretizes the states and the costates over a time grid where they are unknown at discrete points (David Morante (2021)).

Now, each of these approaches and techniques can be solved with several methods: Gradient-based, Heuristic, and Hybrid.

Generally, a gradient-based or deterministic approach starts with an unknown initial state vector \mathbf{x} . The idea is to, iteration per iteration k , update this vector by knowing a search direction p_k and the step length α_k . Then, the next x_{k+1} is computed as $x_{k+1} = x_k + \alpha_k p_k$. A very typical method, in this case, is the Sequential Quadratic Programming or interior point methods (David Morante (2021)).

The heuristic method generates a series of possible solutions which are continuously changing based on stochastic rules. The purpose is to find which solution of all of these has the lowest or highest cost (depending on your optimization goal). Typical heuristic methods are Particle Swarm Optimization (PSO) or Genetic Algorithms (GA) (David Morante (2021)).

Finally, the hybrid method tries to get the best of both worlds between the deterministic methods and heuristic methods. Normally, the heuristic method is used as an algorithm that searches in a large domain of possible solution so while the deterministic method aid to satisfy the constraints of the problem.

Figure 3.5 represents the pros and cons of each approach and method. Flexibility gives an idea of how easy would be to apply the same approach or method to a different problem. Robustness describes the sensitivity of the methods with the initialization and Optimality describes how probable is to find the optimal solution.

		Flexibility	Robustness	Optimality
Numerical approaches	Indirect			
	Direct			
Numerical solutions	Deterministic			
	Heuristic			
	Hybrid			

Figure 3.5: Pros and cons of optimization approaches David Morante (2021)

At first, the problem was going to be solved by using an indirect and heuristic approach with a PSO algorithm, so an optimal solution and flexibility are guaranteed sacrificing robustness. Nevertheless, due to the number of constraints in this problem (see Chapter 4), the study was too complex to converge by just using a heuristic method. So, a final hybrid algorithm was implemented.

Therefore, in the next sections, it is explained the two types of algorithms used to build the hybrid algorithm. A heuristic PSO algorithm and a deterministic SQP algorithm.

3.2.2 Particle Swarm Optimization

The Particle Swarm Optimization (PSO) algorithm is a population-based algorithm that represents the movement of organisms in a bird flock or fish school (Wikipedia (2023e)). This algorithm seems to be equally selected for interplanetary and rendezvous missions as the Genetic Algorithm (GA) (Abolfazl Shirazi (2018)). Nevertheless, although the GA is generally selected as the first choice, the PSO is finally selected due to its easy comprehension and implementation. The PSO algorithm is deeply explained in (A.Conway (2010)), albeit in this section the main concepts are described.

The goal of the PSO algorithm is to obtain the value of a series of n parameters $\mathbf{X} = [x_1, \dots, x_n]$ that optimize the objective function J . This objective function is generally defined, for a constrained optimization problem, in Equation 3.10 where the idea is to define J as the variable to optimize and $\Phi = [\phi_1, \dots, \phi_m]$ the constraint vector of the problem (see also Chapter 4).

$$\tilde{J} = J + \sum_{r=1}^m \Phi \quad (3.10)$$

However, depending on the application, the objective function can be classified as in Figure 3.6. For this problem, the objective function is the fuel consumption.

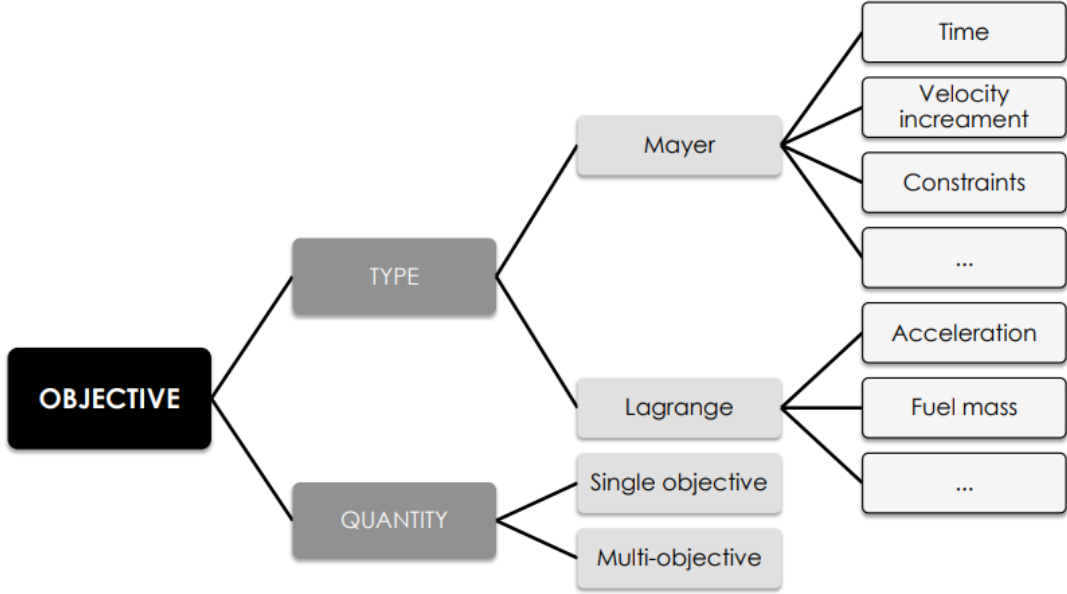


Figure 3.6: Possible objective function definition Abolfazl Shirazi (2018)

As mentioned before, the PSO is a population-based algorithm, so there exists a number of particles N where each particle has associated a vector \mathbf{X} , that is defined as $\mathbf{X}(i)$ where $i = 1, \dots, N$. At the same time, each particle has associated a velocity vector $\mathbf{W} = [w_1, \dots, w_n]$.

For every single particles N , its position vector \mathbf{X} and velocity vector \mathbf{W} is defined within a range expressed in Equation 3.11, where $\mathbf{a} = [a_1, \dots, a_n]$, $\mathbf{b} = [b_1, \dots, b_n]$ and $\mathbf{d} = \mathbf{b} - \mathbf{a}$.

$$\mathbf{a} \leq \mathbf{X} \leq \mathbf{b} \quad -\mathbf{d} \leq \mathbf{W} \leq \mathbf{d} \quad (3.11)$$

Next, there are several steps to apply the PSO algorithm, also considering the number of iterations j .

(1). First, the vector $\mathbf{X}^j(i)$ and $\mathbf{W}^j(i)$ is initialized randomly within its ranges. Then, the objective function is evaluated for every position of each particle i .

(2). Secondly, it is selected the best position that each particle has ever had, defined as $\phi^j(i)$ and also it is selected the best global position \mathbf{Y}^j . The final step is to save the best objective function ever had, corresponding to the particle \mathbf{Y}^j .

(3). Then, the next velocity vector is updated for every single particle $i = 1, \dots, N$.

$$\mathbf{W}^{j+1}(i) = \mathbf{c}_I \mathbf{W}^j(i) + \mathbf{c}_C [\phi^j(i) - \mathbf{X}^j(i)] + \mathbf{c}_S [\mathbf{Y}^j - \mathbf{X}^j(i)] \quad (3.12)$$

where \mathbf{c}_I , \mathbf{c}_C and \mathbf{c}_S are the inertial, cognitive and social weights respectively. These weights are defined in Equation 3.13.

$$\begin{aligned} \mathbf{c}_I &= \frac{1 + \mathbf{r}_1(0, 1)}{2} \\ \mathbf{c}_C &= 1.49445 \mathbf{r}_2(0, 1) \\ \mathbf{c}_S &= 1.49445 \mathbf{r}_3(0, 1) \end{aligned} \quad (3.13)$$

where $\mathbf{r}(0, 1)$ are random vectors from 0 to 1 with a length vector of n . Then, if the velocity vector $\mathbf{W}^{j+1}(i) < -\mathbf{d}$, the new value is $\mathbf{W}^{j+1}(i) = -\mathbf{d}$. The same happens with the upper limit.

(4) Finally, the position vector $\mathbf{X}^{j+1}(i)$ is updated with Equation 3.14.

$$\mathbf{X}^{j+1}(i) = \mathbf{X}^j(i) + \mathbf{W}^j(i) \quad (3.14)$$

For sure, this position should be also limited in case it exceeds its range. Consequently, if $\mathbf{X}^{j+1}(i) < \mathbf{a}$, then $\mathbf{X}^{j+1}(i) = \mathbf{a}$. Moreover, if $\mathbf{X}^{j+1}(i) > \mathbf{b}$, then $\mathbf{X}^{j+1}(i) = \mathbf{b}$.

As the values of the position vector and the velocity vector are again known, this process is repeated till the maximum number of iterations is achieved.

3.2.3 Sequential Quadratic Programming

Sequential Quadratic Programming (SQP) is a method for solving constrained nonlinear optimization problems. In this case, the SQP computes a sequence of problems where each problem is solved as a problem of Quadratic Programming (QP). Hence, the idea behind this algorithm is to define the optimality conditions and solve them so a final optimal solution is obtained. This is the chosen deterministic method as it has also been used for spacecraft trajectory optimization (Betts (2000)) and it is already implemented in the *fmincon* function in MATLAB (MATLAB (2023b)).

Generally, the goal is to find the state vector of the problem \mathbf{x} that optimizes the equation $F(\mathbf{x})$. As it is a constrained problem, there also exists equality constraints or inequality constraints $\Phi(\mathbf{x})$. At this point, to guarantee an optimal solution, the Karush-Kuhn-Tucker (KKT) equations are defined as optimality conditions for the problem (MATLAB (2023a)). This condition is defined in Equation 3.15, where $\boldsymbol{\lambda}$ are the Lagrange multipliers and $L = F(\mathbf{x}) + \Phi(\mathbf{x})^T \boldsymbol{\lambda}$ is the Lagrangian.

$$\nabla L(\mathbf{x}, \boldsymbol{\lambda}) = 0 \quad (3.15)$$

The purpose is to solve this condition by using a first-order approximation of the previous expression. This first-order expression is defined in Equation 3.16.

$$\nabla L(\mathbf{x}, \boldsymbol{\lambda}) = \nabla L(\mathbf{x}_0, \boldsymbol{\lambda}) + \nabla^2 L(\mathbf{x}_0, \boldsymbol{\lambda}) \begin{pmatrix} \delta \mathbf{x} \\ \delta \boldsymbol{\lambda} \end{pmatrix} \quad (3.16)$$

By using this first approximation and the KKT condition, a final system of equations defined in Equation 3.17 can be stated.

$$\begin{bmatrix} \nabla^2 L(\mathbf{x}_0, \boldsymbol{\lambda}) & N \\ N & 0 \end{bmatrix} \begin{bmatrix} \delta \mathbf{x} \\ \delta \boldsymbol{\lambda} \end{bmatrix} = - \begin{bmatrix} \nabla L(\mathbf{x}, \boldsymbol{\lambda}) \\ \boldsymbol{\Phi}(\mathbf{x}) \end{bmatrix} \quad (3.17)$$

Finally, by solving this system of equations, the value of the state vector and Lagrange multipliers for the next iteration $k + 1$ is calculated as in Equation 3.18.

$$\begin{bmatrix} \mathbf{x}_{k+1} \\ \boldsymbol{\lambda}_{k+1} \end{bmatrix} = \begin{bmatrix} \mathbf{x}_k \\ \boldsymbol{\lambda}_k \end{bmatrix} + \begin{bmatrix} \delta \mathbf{x} \\ \delta \boldsymbol{\lambda} \end{bmatrix} \quad (3.18)$$

The final result is obtained once the solution has converged or it has exceeded the maximum number of iterations.

Chapter 4

Methodology

This chapter explains the procedure and real implementation of the PSO and SQP algorithms into a real application, in this case, low-thrust spacecraft trajectory optimization.

Section 4.1 describes the most complete problem subsequently applied to a mission to Mars, where the goal is to optimize the fuel consumption by fixing the time of flight t_f . In this part, it is also defined the pre-step needed for converging the fuel-optimal problem known as the Energy-optimal problem (homotopic approach). Then in Section 4.2, the time-optimal problem based on its reduced complexity compared with the previous one is introduced as the problem that validates the PSO algorithm. Finally, Section 4.3 shows the algorithm and explains in more detail the procedure to obtain the final result.

4.1 Fuel-optimal problem with Homotopic approach

4.1.1 Introducing the dynamic and conditions of the system

When the goal is to minimize fuel consumption by finding the optimal control variables, the problem statement should start with the differential equations shown in Equation 4.1. As a reminder, these expressions compute the dynamics of the spacecraft.

$$\begin{aligned}\dot{\mathbf{v}} &= -\frac{\mu}{r^3}\mathbf{r} + \frac{T_{max}u}{m}\boldsymbol{\gamma} \\ \dot{\mathbf{r}} &= \mathbf{v} \\ \dot{m} &= -\frac{T_{max}u}{g_0 I_{sp}}\end{aligned}\tag{4.1}$$

Considering the previous set of equations, the state vector and the control vector are expressed in Equation 4.2. Where \mathbf{r} and \mathbf{v} are the position and the velocity vector in 3D, m and T_{max} are the mass and the thrust of the spacecraft respectively, I_{sp} is

the thruster specific impulse, $\boldsymbol{\gamma}$ is the thruster angle vector and u is the variable that weighs the maximum value of the Thrust between $[0, T_{max}]$.

$$\begin{aligned}\boldsymbol{x} &= [\boldsymbol{r}, \boldsymbol{v}, m] \\ \boldsymbol{u} &= [\boldsymbol{\gamma}, u]\end{aligned}\tag{4.2}$$

In order to obtain the solution from these equations, it would be strictly necessary to establish the initial conditions, the time of flight t_f , the final position and velocity conditions, and the control law during the integration time. The initial conditions are defined by knowing in advance the flight's initial date and time. The mass, in this case, is dimensionless by the initial mass of the spacecraft. Finally, the final position and velocities are known as the t_f is also fixed.

Equations 4.3 to 4.6 are the conditions needed for solving the problem. As can be seen, the final mass is free, which means it would be automatically computed once the integration has been performed.

$$\boldsymbol{r}(t_0) = \boldsymbol{r}_0 \qquad \boldsymbol{r}(t_f) = \boldsymbol{r}_f \tag{4.3}$$

$$\boldsymbol{v}(t_0) = \boldsymbol{v}_0 \qquad \boldsymbol{v}(t_f) = \boldsymbol{v}_f \tag{4.4}$$

$$m(t_0) = 1 \qquad m(t_f) = \text{free} \tag{4.5}$$

$$t(t_0) = 0 \qquad t(t_f) = t_f \tag{4.6}$$

As illustrated, this problem needs to satisfy, at least, six constraints that can be seen in Equation 4.7. These constraints exist based on the nature of the problem, where the goal is to arrive at a specific point in the space (rendezvous).

$$[\boldsymbol{r}(t_f) - \boldsymbol{r}_f, \boldsymbol{v}(t_f) - \boldsymbol{v}_f] = 0 \tag{4.7}$$

4.1.2 Calculating the optimal control

Before explaining how the optimal control is obtained, it is essential to show the objective function. This objective function defines the variable to optimize. The first term of Equation 4.8 represents the homotopic transformation of the fuel consumption meanwhile the second term shows the constraints of a rendezvous problem and the transversality condition to accomplish (Jiang (2012)).

$$\begin{aligned}\tilde{J} &= \frac{T_{max}}{I_{sp}g_0} \int_{t_f}^{t_0} [u - \epsilon u(1 - u)] dt + [\mathbf{r}(t_f) - \mathbf{r}_f, \mathbf{v}(t_f) - \mathbf{v}_f, \lambda_m(t_f)] \\ &= \int_{t_f}^{t_0} L dt + \Phi\end{aligned}\tag{4.8}$$

Now, to get the optimal law, the control vector \mathbf{u} must be calculated so the objective function is minimized. For this, the fuel-optimal problem has the characteristic of a two-point boundary-value problem (TPBVP) by using the PMP (Tieding Guo (2011)).

As defined in A.Conway (2010), the PMP establishes that if the control vector minimizes the Hamiltonian, the trajectory will be optimal. This Hamiltonian is defined in Equation 4.9, where L is the first term of the objective function in Equation 4.8, $\boldsymbol{\lambda}$ is the costate vector $\boldsymbol{\lambda} = [\boldsymbol{\lambda}_r, \boldsymbol{\lambda}_v, \lambda_m]$ and f is the dynamic of the spacecraft in Equation 4.1.

$$H = L + \boldsymbol{\lambda}^T f\tag{4.9}$$

So, the control vector must be computed in such a way that minimizes the variable H . The costate vector $\boldsymbol{\lambda}$ dynamic is calculated as shown in Equation 4.10.

$$\dot{\boldsymbol{\lambda}} = - \left(\frac{\partial H}{\partial \mathbf{x}} \right)\tag{4.10}$$

The vector \mathbf{x} dependence with time is shown in Equation 4.11 and its definition was presented in Equation 4.2.

$$\dot{\mathbf{x}} = \mathbf{f}(\mathbf{x}, t, \mathbf{u})\tag{4.11}$$

With all this explained, we can come back to the second term of the objective function in Equation 4.8. Next to the position and velocity constraints, there is one term of the costate vector, which is λ_m . This costate term appears thanks to the transversality condition. The transversality condition in a PMP problem establishes that if the boundary of a state in \mathbf{x} is free, the corresponding costate boundary is zero. Then, considering the Equation 4.5 where the mass at t_f is free, it can be stated that $\lambda_m(t_f)$ needs to be zero.

Finally, all the constraints of the problem are presented in Equation 4.12.

$$\Phi = [\mathbf{r}(t_f) - \mathbf{r}_f, \mathbf{v}(t_f) - \mathbf{v}_f, \lambda_m(t_f)] = 0\tag{4.12}$$

Normally, when the problem is not constrained, the objective function lacks the second term. Nevertheless, when the problem requires a constrained optimization, the constraints are added as a penalty function so they can be optimized and reduced to zero. However, there are other ways to take this into account (Tieding Guo (2011)).

Continuing with the PMP, if the Hamiltonian function in Equation 4.9 is expanded, Equation 4.13 is obtained.

$$H = \boldsymbol{\lambda}_r \cdot \mathbf{v} + \boldsymbol{\lambda}_v \cdot \left(-\frac{\mu}{r^3} \mathbf{r} + \frac{T_{max} u}{m} \boldsymbol{\gamma}\right) - \lambda_m \frac{T_{max}}{I_{sp} g_0} u + \frac{T_{max}}{I_{sp} g_0} [u - \epsilon u(1 - u)] \quad (4.13)$$

Considering this, the next step is to define the dynamic of the costate vector $\boldsymbol{\lambda}$ and then define the control variables so the Hamiltonian is optimized. So, the dynamic of $\boldsymbol{\lambda}$ can be seen in Equation 4.14 by using the Hamiltonian in Equation 4.13 and applying Equation 4.10.

$$\begin{aligned} \dot{\boldsymbol{\lambda}}_r &= \frac{\mu}{r^3} \boldsymbol{\lambda}_v + \frac{3\mu \mathbf{r} \cdot \boldsymbol{\lambda}_v}{r^5} \mathbf{r} \\ \dot{\boldsymbol{\lambda}}_v &= -\boldsymbol{\lambda}_r \\ \dot{\lambda}_m &= -\frac{T_{max} u}{m^3} |\boldsymbol{\lambda}_v| \end{aligned} \quad (4.14)$$

From the expression in Equation 4.13, the thrust pointing unit vector should be contrary to the direction of $\boldsymbol{\lambda}_v$ to reduce the result of the multiplication $\boldsymbol{\lambda}_v \cdot \boldsymbol{\gamma}$ and minimize the Hamiltonian. This statement is defined in Equation 4.15.

$$\boldsymbol{\gamma} = -\frac{\boldsymbol{\lambda}_v}{|\boldsymbol{\lambda}_v|} \quad (4.15)$$

Regarding the value of u , the condition 4.16 shows the values that this variable should have depending on the expression m in Equation 4.17.

$$u = \begin{cases} u = 0, & \text{if } m > \epsilon \\ u = 1, & \text{if } m < -\epsilon \\ u = \frac{1}{2} - \frac{m}{2\epsilon}, & \text{if } |m| \leq \epsilon \end{cases} \quad (4.16)$$

$$m = 1 - \frac{I_{sp} g_0 |\boldsymbol{\lambda}_v|}{m} - \lambda_m \quad (4.17)$$

This condition and expression m can be obtained by reorganizing the terms that multiply $\frac{T_{max}}{I_{sp}g_0}$ in the Hamiltonian. By using the operation $\frac{\delta}{\delta u} = 0$ in these terms, it is finally obtained the relation $u = 1/2 - m/(2\epsilon)$.

4.1.3 The homotopic approach

Right at the beginning of the Subsection 4.1.2, the first term of the objective function in Equation 4.8 and the condition in 4.16 has a term ϵ . This parameter introduces what is called the homotopic approach. This method has been previously used in Jiang (2012) and Tieding Guo (2011) for Spacecraft Trajectory Optimization and it is deeply explained in R. Bertrand (2002).

First, it can be seen that if $\epsilon = 0$, the first term of the objective function represents the fuel consumption. Nevertheless, if $\epsilon = 1$, the first term is defined as Equation 4.18. If this problem is solved, the final solution represents an Energy-optimal value.

$$J = \frac{T_{max}}{I_{sp}g_0} \int_{t_f}^{t_0} u^2 dt \quad (4.18)$$

The Energy-optimal problem is presented here as a way to define a continuous control law and increase the convergence radius of the problem. If $\epsilon = 0$, the condition in 4.16 forces the thrust to value 0 or T_{max} . This is called a bang-bang control, and it is extremely difficult to converge. Hence, the Energy-optimal problem is computed to improve the convergence behavior and then, its solution is used to finally calculate the Fuel-optimal problem.

This section has explained the procedure to define the fuel-optimal problem for a rendezvous mission where a more clear explanation of how it is calculated can be seen in Section 4.3. Nevertheless, there are other problems such as the Time-optimal problem in Section 4.2 which is presented as a method to validate part of the code.

4.2 Time-optimal problem

The PSO algorithm is the key to the Fuel-optimal problem presented in this Thesis. Nevertheless, this mathematical approach must be validated previously. Hence, the time-optimal problem is the tool that validates the PSO algorithm and, consequently, increases the veracity of the code.

For this case, the idea is to optimize the spacecraft trajectory where several assumptions have been made and follow the structure of the Optimal Low-thrust Optimal Transfers problem presented by A.Conway (2010).

The goal of the study is to optimize the time of flight t_f for an orbital transfer between two different 2D circular orbits, where the objective function changes to $J = t_f$. As it is still a continuous optimal control problem, the approach for getting the expressions of the costates as well as their relation with the control variables is exactly the same as in the previous section. For a further explanation and development of the problem, you can see it in A.Conway (2010).

In any case, there are still important aspects to consider that differentiate both problems. First of all, the transversality conditions are different as the time of flight t_f is an unknown for this case (free). The time transversality conditions should be considered as a constraint as presented in the previous section. Nevertheless, Conway demonstrates it is possible to eliminate this expression from the constraints based on the homogeneous properties of the costates equations $\boldsymbol{\lambda}$ in Equation 4.19 .

$$\begin{aligned}\dot{\lambda}_1 &= -\lambda_3 + \frac{x_2\lambda_2}{x_3} \\ \dot{\lambda}_2 &= \frac{-2\lambda_1x_2 + x_1\lambda_2}{x_3} \\ \dot{\lambda}_3 &= \frac{\lambda_1x_2^2 - x_1x_2\lambda_2}{x_3^2} - \frac{2\mu\lambda_1}{x_3^3}\end{aligned}\tag{4.19}$$

As can be seen, the vector $\boldsymbol{\lambda}$ is defined this time as $[\lambda_1, \lambda_2, \lambda_3]$, reducing its length based on the less number of differential equations that describe the dynamic of the system (2D problem). Finally, the position of the particle is redefined as $[\lambda_1(t_0), \lambda_2(t_0), \lambda_3(t_0), t_f]$ revealing that the time of flight t_f is directly searched on the algorithm meanwhile the fuel consumption of the previous problem is not considered in the particle's position. The results using this approach can be seen in Chapter 5

Once both problems have been explained, the algorithm structure is presented for a more clear explanation of how the Fuel-optimal problem is solved.

4.3 Algorithm structure

In this section, the goal is to provide the logic behind the code created for solving the Fuel-optimal problem. Therefore, a more detailed explanation of the procedure is expected. Although the PSO algorithm is used as the only algorithm that provides the optimal solution for the Time-optimal problem, for the optimization of fuel consumption it is needed to implement and hybrid algorithm due to its complexity.

The flowchart in Figure 4.1 shows the code structure and logic to solve the problem.

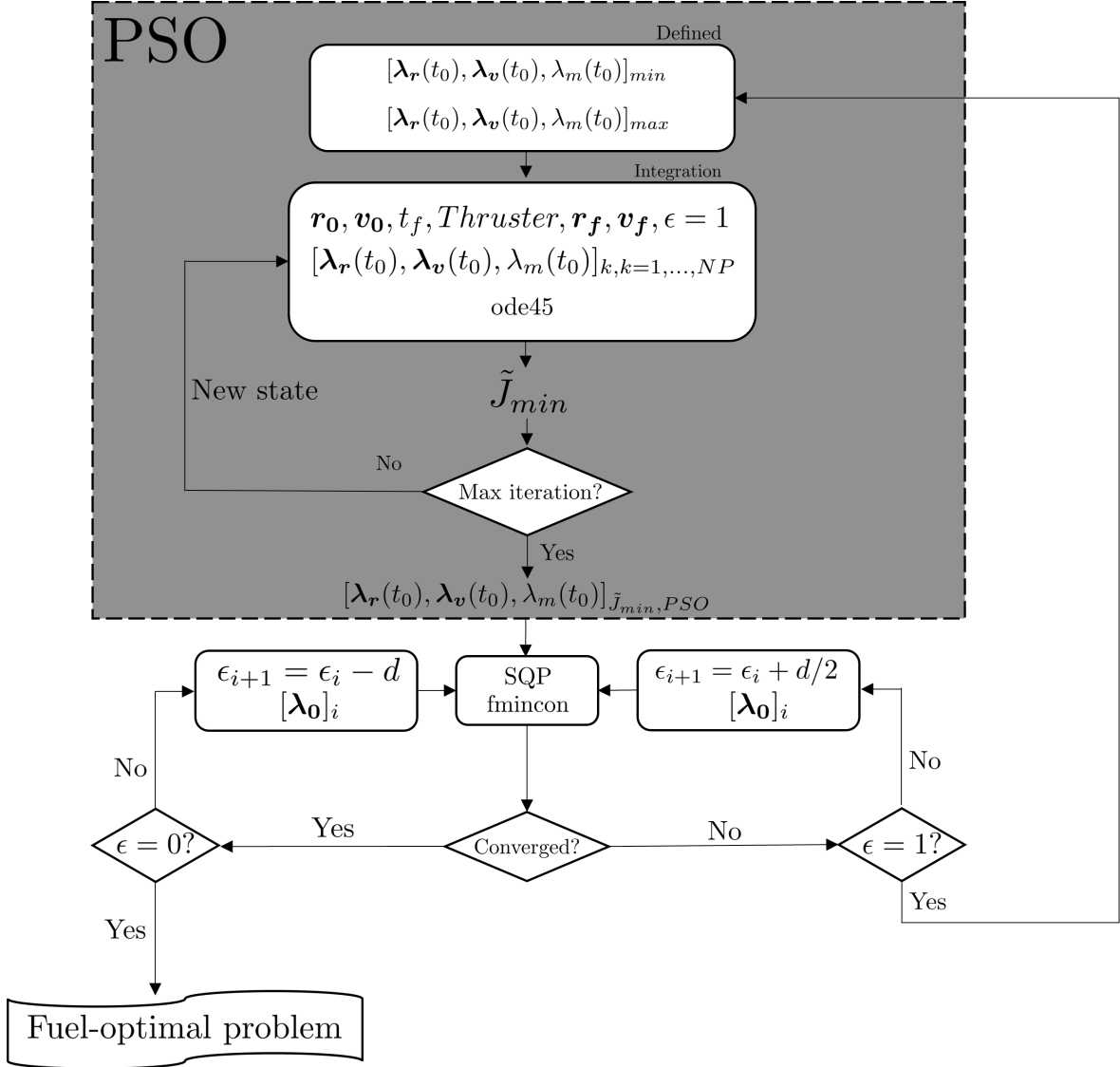


Figure 4.1: Flowchart for the Fuel-optimal problem

First, the PSO algorithm is used to initialize the optimization process continued by the SQP. At the beginning of the study, it was attempted to obtain also the fuel-optimal solution by just implementing the PSO, however, the number of constraints (seven in total) made it very difficult to converge and provide a reduced rendezvous error. It is also mentioned by other authors in Jiang (2012).

Hence, the PSO with $\epsilon = 1$ is used as an initialization as in Jiang (2012) to reduce the objective function in Equation 4.8 as much as possible. The final \tilde{J}_{min} depends on the minimum $[\lambda_r(t_0), \lambda_v(t_0), \lambda_m(t_0)]_{min}$ and maximum $[\lambda_r(t_0), \lambda_v(t_0), \lambda_m(t_0)]_{max}$ particle position, as well as the number of iteration and particles established in the problem.

Once the particle's position is defined for all the particles, the process follows the

steps of the PSO algorithm explained in Section 3.2.2. Basically, the idea is to integrate for every single position of each particle k the equation of motions in Equation 4.1 as well as the costates equation in Equation 4.10. Then, the \tilde{J} is computed as in equation 4.8. The algorithm used for the integration is the function implemented in MATLAB named `ode45`, which uses the Dormand-Prince method belonging to the family of Runge-Kutta. The function `ode45` is the typical solver that is normally used in all engineering applications. Due to its good performance for this problem, it was not needed to test any other solver.

Following the PSO logic, the algorithm will be calculating these particle's positions for every single iteration and comparing what is the position or initial state of $\boldsymbol{\lambda}$ that minimizes the expression of \tilde{J} . The final \tilde{J}_{min} used for initializing the SQP function implemented in MATLAB depends on the maximum iteration defined in the PSO algorithm. This maximum value is defined considering the maximum value of \tilde{J}_{min} that provides an enough good initialization for the SQP algorithm. This number of iterations has been tested by trial and error process also considering the computation time.

The next part of the algorithm uses the Sequential Quadratic Programming (SQP) implemented in the function `fmincon` in MATLAB. Hence, for solving the problem it is implemented a hybrid algorithm using both, an heuristic method (PSO) and the Gradient-based method (SQP). In fact, this approach is normally used for cases where it is needed to explore a large design domain (using heuristic methods as PSO) and then satisfy the constraints by using the Gradient-based method (SQP) (David Morante (2021)). This is the reason why the final results were finally obtained by implementing the Gradient-based method due to the impossibility of using only the PSO as previously mentioned.

For obtaining the final result, the Energy-optimal problem is computed with $\epsilon = 1$. If it converges, the ϵ is decreased by a value of d and the initial value of the costates $[\boldsymbol{\lambda}_0]_i$ is used as initialization for the new ϵ_{i+1} . In case $\epsilon = 1$ does not converge, the PSO is re-started to improve the value of \tilde{J} .

There is also the possibility that $\epsilon < 1$ and it does not converge. In this case, the new value for ϵ is valued as the average of the previous ϵ value that converged, and the new that did not converge. Then, as the ϵ is closer to the ϵ that converged, there are higher probabilities of convergence.

The definition of convergence represents always that the rendezvous error is smaller than a limit and the transversality condition has been properly satisfied. The definition of rendezvous error is on Equation 4.20.

$$e = 100 \frac{[\mathbf{r}(t_f) - \mathbf{r}_f, \mathbf{v}(t_f) - \mathbf{v}_f]}{[\mathbf{r}_f, \mathbf{v}_f]} \quad (4.20)$$

During the algorithm, the maximum error e for the position and the velocity is $e < 5\%$, and λ_m should always be between $[-0.001, 0.001]$. Finally, when $\epsilon = 0$ and it converges, the Fuel optimal problem has been calculated.

During Section 4 it has been explained the procedure and theory to calculate a Time-optimal problem as well as a complex Fuel-optimal problem. In the next Chapter 5 the purpose is to show the results of both problems and to analyze the data.

Chapter 5

Results

The purpose of this section is to present the validation of the algorithm previously described as well as solve a real impulsive mission in order to compare the advantages or disadvantages of using a low-thrust thruster.

5.1 PSO Validation

The hybrid algorithm presented in Section 4.3 starts with the PSO. For this reason, in order to make sure the initialization is properly calculated, it is necessary to validate the PSO implementation.

The methodology behind the problem used for the validation is explained in Section 4.2. This problem requires less complexity as it is an optimization problem with 2D circular orbits. Therefore, it is possible to obtain a final solution by using the PSO as the main algorithm and not as initialization.

In Table 5.1 can be seen the comparison between the results obtained by Conway in A.Conway (2010) and this study.

The initial position of the initial planet and the final position of the final planet are defined by the radius of their orbits, R_1 and R_2 . The effective exhaust velocity c and thrust-to-mass ratio n_0 meaning is better understood in Equation 5.1. Here, T is the thrust, m is the mass of the spacecraft, m_0 is the initial mass of the spacecraft, t is the time, and t_0 is the initial time.

The effective exhaust velocity corresponds to the thrust generated per unit of propellant mass flow rate. In the same way, the thrust-to-mass ratio n_0 is the initial thrust per unit mass of spacecraft.

$$\frac{T}{m} = \frac{T}{m_0 - \frac{T}{c}(t - t_0)} = \frac{cn_0}{c - n_0(t - t_0)} \quad (5.1)$$

$$n_0 = \frac{T}{m_0}$$

Finally, the units in this problem are presented in DU and TU , which are the distance between the Earth and the Sun ($1.495978707 \cdot 10^8$ km) and the time needed to have a standard gravitational parameter μ equal to $1 \text{ DU}^3/\text{TU}^2$ ($5.022642 \cdot 10^6$ s).

	A.Conway (2010)	Study
Initial radius $R_1[DU]$	1	1
Final radius $R_2[DU]$	2	2
Effective exhaust velocity $c [DU/TU]$	1.5	1.5
Initial thrust-to-mass ratio $n_0 [DU/TU^2]$	0.01	0.01
Time of flight $t_f [TU]$	27.970	27.968

Table 5.1: PSO validation

As it was explained in section 4.2, the goal is to minimize the time of flight t_f . As the solution error is 0.007 %, the PSO is considered as validated.

It is also interesting to see how \tilde{J} (the objective function considering the rendezvous constraints) in Figure 5.1 decreases with the number of iterations. In this case, the number of particles used is 50 and the maximum number of iterations is 1000. If a more accurate solution is needed, the number of iterations should increase.

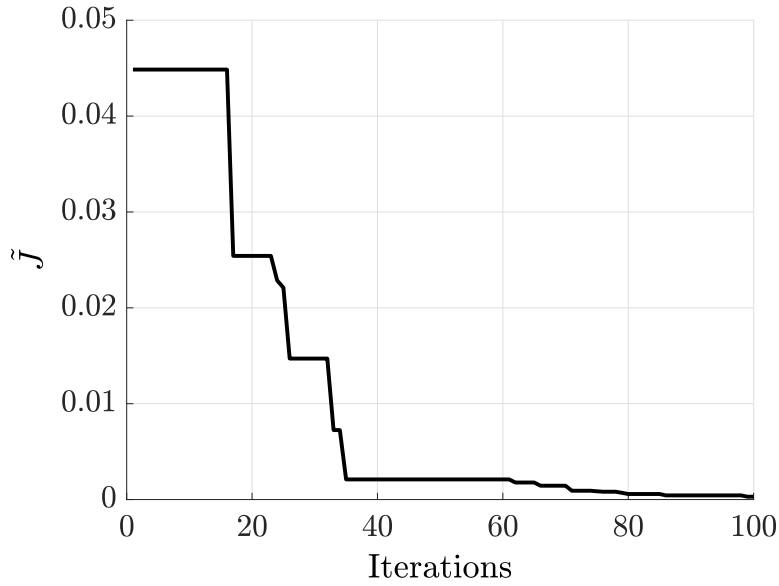


Figure 5.1: PSO validation - Objective function vs Iteration

Finally, the costates of λ (or adjoint variables) are presented in Figure 5.2 (a). Comparing these results with the ones obtained by Conway in Figure 5.2 (b), it can be concluded one more time that the PSO algorithm is validated.

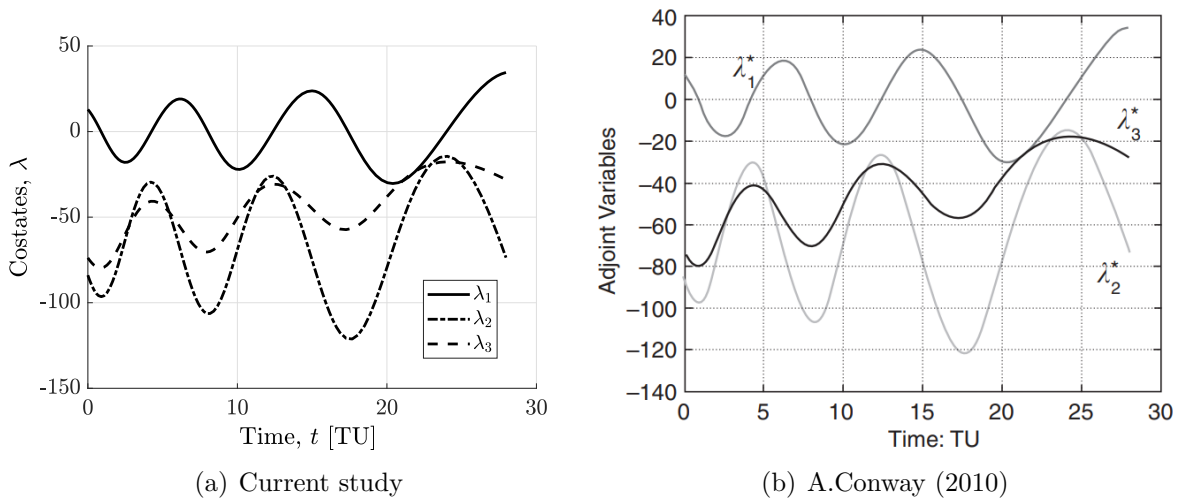


Figure 5.2: PSO validation - Costates vs Time

5.2 Hybrid algorithm validation

For the hybrid algorithm, the problem statement defined in Section 4.1 shows a more complex problem where this time, the orbits are described in Equation 4.1.

Table 5.2 shows the problem that is replicated for the validation. In this case, the goal is to minimize the fuel consumption for an interplanetary rendezvous between Earth and Venus, at a fixed initial date and time of flight t_f .

	Jiang (2012)	Study
Initial date	October 7, 2005	October 7, 2005
Time of flight t_f [days]	1000	1000
Maximum thrust T_{max} [N]	0.33	0.33
Specific impulse I_{sp} [s]	3800	3800
Initial mass m_0 [kg]	1500	1500
Final mass m_f [kg]	1290.58	1296.47

Table 5.2: Hybrid algorithm validation

The solution relative error between Fanghua Jiang's study and the current study is 0.46 %. Hence, the hybrid algorithm is considered validated. Nevertheless, it is important to verify that the rendezvous error is below the maximum established by the algorithm (5 %). The error expression is in Equation 4.20.

Table 5.3 shows how the maximum error is successfully accomplished.

Rendezvous error	e_{r_x}	e_{r_y}	e_{r_z}	e_{v_x}	e_{v_y}	e_{v_z}
Value	2.9 %	1.4 %	1.3 %	0.4 %	1.7 %	2.2 %

Table 5.3: Hybrid algorithm validation - Error rendezvous

Figure 5.3 shows how \tilde{J} is reduced with the iterations during the PSO initialization. In this case, the number of particles is 40 and the maximum number of iterations is 1000. These numbers have been defined with the same order of magnitude as the references Jiang (2012). In any case, these values should be changed in order to get a proper solution within a relatively reduced computational time.

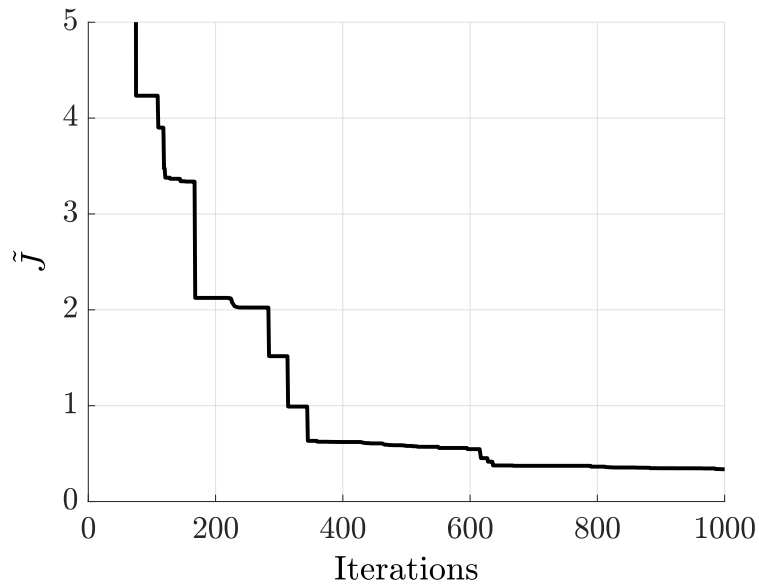


Figure 5.3: Hybrid algorithm validation - Objective function vs Iteration

As in the previous section, the current problem also needs to compute the costate vector λ . Figure 5.4 shows the different costate values for each state of the system. As can be seen, the transversality condition $\lambda_m = 0$ is accomplished at the end of the integration. These results are comparable with the ones obtained in Tieding Guo (2011).

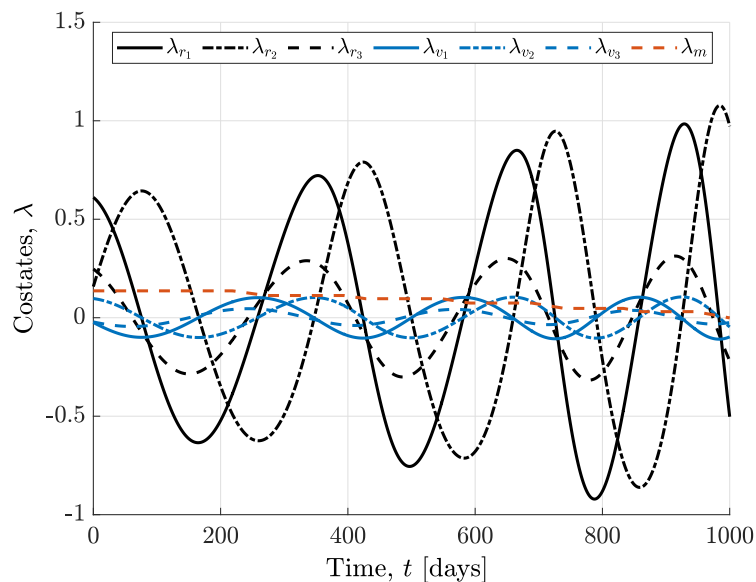


Figure 5.4: Hybrid algorithm validation - Costates vs Time

Once the optimal solution has been calculated, the continuous low-thrust thruster is switched on and off depending on the Equation 4.16. The repetitive thrust distribution in Figure 5.5 causes the decrement of the spacecraft's mass in Figure 5.5. Due to the same value of thrust during each interval, the decrement rate is equal.

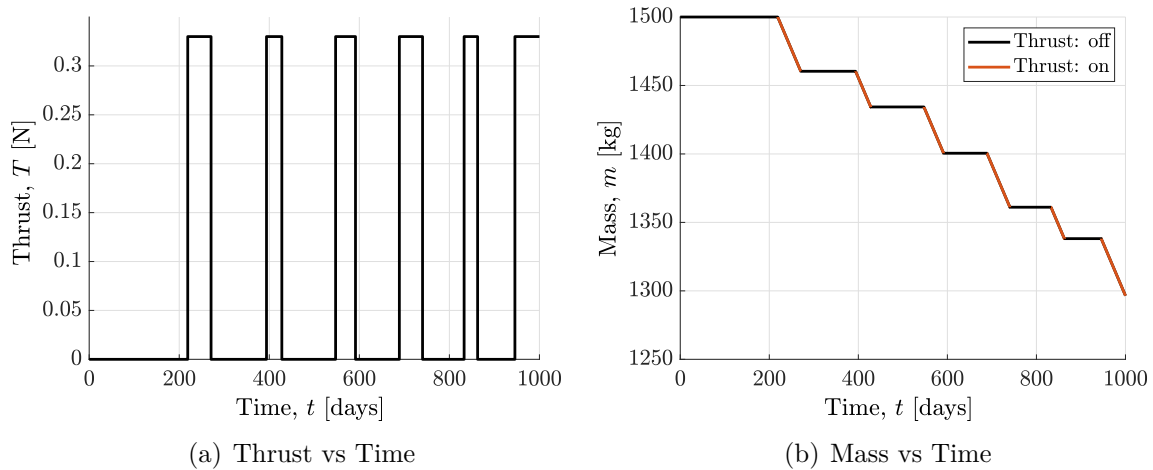


Figure 5.5: Hybrid algorithm validation - Thrust and Mass vs Time

Considering the thrust distribution of Figure 5.5, it can be predicted the shape of the orbital trajectory in Figure 5.6. As the spacecraft orbits the sun several times, the thruster is switched on and off frequently.

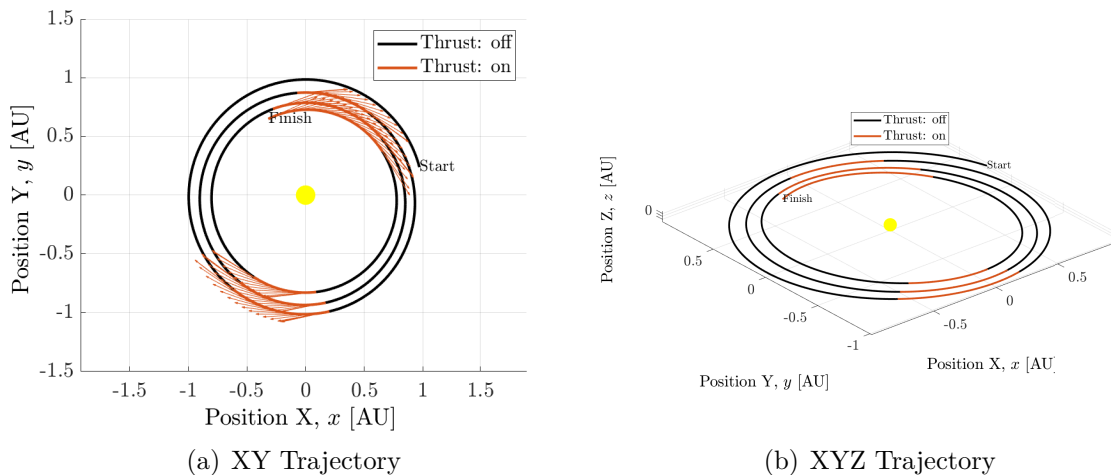


Figure 5.6: Hybrid algorithm validation - Orbital trajectory

Figure 5.6 also demonstrates a logical behavior about the thruster pointing direction defined by the arrows. In order to arrive on Venus, the thruster must point in the opposite direction of the spacecraft's movement direction. If it does not happen,

the spacecraft will never arrive on Venus as it will increase its distance from the planet.

5.3 Real mission comparison

Once the algorithm has been validated, it is time to prove if a continuous low-thrust trajectory has some advantage compared with trajectories where impulsive engines are used.

For this, the Mars Orbiter Mission (MoM) has been selected. The MoM mission was launched on November 5, 2013, and started its journey to Mars on November 23, 2013. The idea is to compare if the fuel consumption computed by the algorithm is lower than the fuel consumption of the real mission. The engine and spacecraft values has been obtained from W.Andrew Hoskings & M.Monheiser (2007) and NASA (2023b). For the low-thrust problem, the initial mass has been calculated by removing the 852 kg of propellant from the MoM mission and adding the weight of two NEXT-C engines, one tank, and the maximum capacity of this tank. Furthermore, the MoM's trajectory data has been collected from the NASA web page (Jet Propulsion Laboratory (2023)).

Table 5.4 presents the final result of the study. Here, the propellant mass consumed is 155.09 kg. This value is the 18 % of the propellant mass initially considered for the MoM.

	Mars Orbiter Mission (MoM)	Study
Initial date	November 23, 2013	November 23, 2013
Time of flight t_f [days]	298	298
Maximum thrust T_{max} [N]	440	0.47
Specific impulse I_{sp} [s]	-	4190
Initial mass m_0 [kg]	1340 (852 of propellant)	958.14
Final mass m_f [kg]	-	803.05

Table 5.4: Real mission comparison

As no data has been found regarding the mass expended during the real mission, it is not possible to conclude with 100 % certainty that a continuous low-thrust trajectory can minimize the fuel consumption. Nevertheless, a continuous low-thrust model could have been a better solution for this mission.

The rendezvous error this time is below 1 % as seen in Table 5.5.

Rendezvous error	e_{r_x}	e_{r_y}	e_{r_z}	e_{v_x}	e_{v_y}	e_{v_z}
Value	0.82	0.40	0.87	0.71	0.45	0.99

Table 5.5: Real mission comparison - Error rendezvous

This time, the thrust profile is different. As the trajectory is simpler, it is only needed to switch on and switch off one time the thrusters. Figure 5.7 (a) also compares the results with different values of ϵ . When a value of $\epsilon = 1$ is considered, the Energy-optimal solution gives a more continuous thrust profile that fosters the increment of the convergence radius. When $\epsilon = 0$, the solution shows a typical bang-bang control (minimum and maximum thrust values). As expected, the propellant mass only decreases when the thruster is switched on.

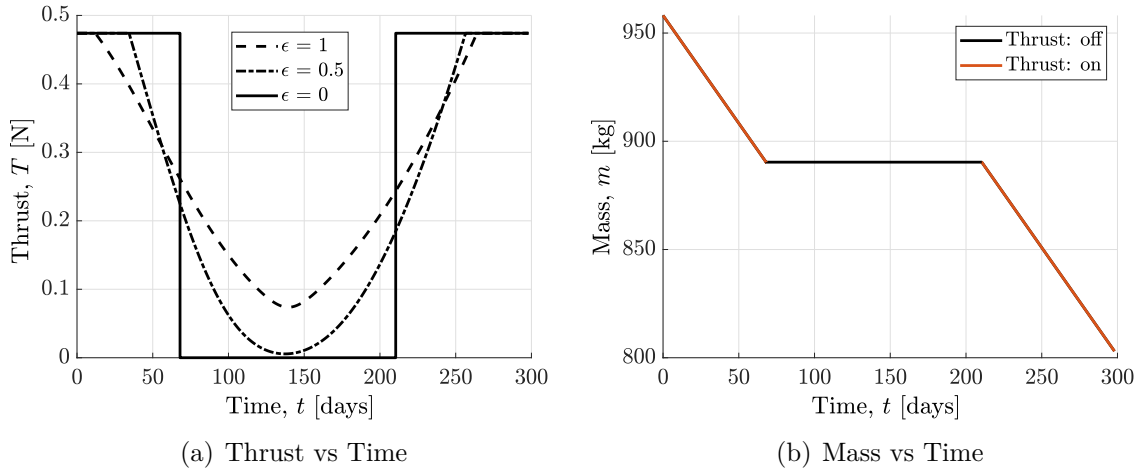
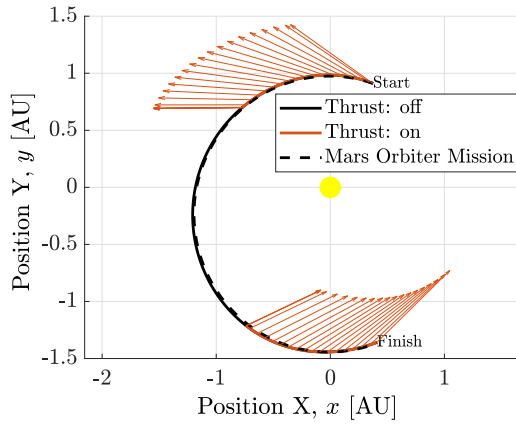
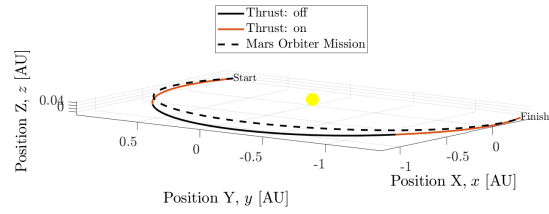
**Figure 5.7:** Real mission comparison - Thrust and Mass vs Time

Figure 5.8 (a) manifests a thruster vector oriented to the spacecraft movement direction in order to increase the distance from the Sun and draw the proper trajectory to Mars. As illustrated, the thruster vector is not parallel to the trajectory's tangent because of its reduced thrust value. Consequently, the vector must point slightly to the right at the beginning of the trajectory so it can increase the distance from the Sun and follow the optimal trajectory. Furthermore, it also happens when arriving on Mars. If the thruster does not point to the left of the trajectory's tangent, the spacecraft will not be able to arrive at the planet and it will pass by to the right of Mars.



(a) XY Trajectory



(b) XYZ Trajectory

Figure 5.8: Real mission comparison - Orbital trajectory

Finally, there seems to be a slight difference on Position Z between these two trajectories in Figure 5.8 (b). The reason could be the presence of perturbations in NASA's data. These perturbations have not been included in the dynamic of the system in Equation 4.1 because of excess complexity.

This section has presented and analyzed the validation results as well as applied the algorithm for a real mission. Section 6 concludes the study and mentions possible future studies.

Chapter 6

Conclusions and future studies

Several conclusions are obtained from this study. Regarding the algorithm, a pure heuristic algorithm such as PSO has not been valid for solving the complex problem of interplanetary rendezvous in 3D dimensions and elliptic orbits. The main reason for this is the number of constraints on the problem. When running a PSO for solving this problem, neither the rendezvous nor the transversality conditions are satisfied within the acceptable errors. For this reason, the final algorithm has a hybrid architecture. Moreover, heuristic algorithms have the nature of computing different results each time. Hence, these algorithms must be run several times, not only for getting reasonable results but also for increasing the chance of getting a globally optimal solution.

Considering the real mission application, the expended mass during the continuous low-thrust trajectory is 18 % of the initial propellant mass considered on the real mission. Therefore, a low-thrust trajectory could be a better solution for interplanetary missions between Earth and Mars. Nevertheless, there is not a 100 % certainty due to a lack of data regarding the mass expended in the real mission.

For future studies, the purpose is to implement a multi-objective algorithm that generates a Pareto frontier to compare the optimal time of flight versus optimal fuel consumption. Furthermore, it would be also interesting to consider perturbations in the system and analyze what is the performance when other deterministic and heuristic algorithms are implemented.

Bibliography

- Abolfazl Shirazi, J. L., Jose Ceberio. (2018). Spacecraft trajectory optimization: A review of models, objectives, approaches and solutions.
- A.Conway, B. (2010). *Spacecraft trajectory optimization*.
- Anne Schattel, M. K. C. B., Mitja Echim. (2016). Low thrust trajectory optimization for autonomous asteroid rendezvous missions.
- Bastida Pertegaz, E. (2021). *Use of the genetic algorithm for the multi-objective optimisation of direct impulsive trajectories between the earth and mars* .
- Betts, J. T. (2000). Very low-thrust trajectory optimization using a direct sqp method.
- Curtis, H. D. (2020). *Orbital mechanics for engineering students*.
- David Morante, M. S., Manuel Sanjurjo Rivo. (2021). A survey on low-thrust trajectory optimization approaches.
- Fernando Alonso Zotes, M. S. P. (2011). Particle swarm optimisation of interplanetary trajectories from earth to jupiter and saturn.
- Frederiksen, J. D. (2021). *Interior point optimization of low-thrust spacecraft trajectories* .
- Hintz, G. R. (2015). *Orbital mechanics and astrodynamics. techniques and tools for space missions*.
- Jet Propulsion Laboratory, N. (2023). *Horizons system*. Retrieved from <https://ssd.jpl.nasa.gov/horizons/app.html#/>
- Jiang, F. (2012). Practical techniques for low-thrust trajectory optimization with homotopic approach.
- Jiang Xiao-yong, Z. H.-b. T. G.-j., LIAN Yi-jun. (2013). A multi-impulse extended method for low - thrust trajectory optimization.
- Koks, D. (2017). *Changing coordinates in the context of orbital mechanics*.

- MATLAB. (2023a). *Algoritmos de optimización no lineal con restricciones*. Retrieved from <https://es.mathworks.com/help/optim/ug/constrained-nonlinear-optimization-algorithms.html>
- MATLAB. (2023b). *fmincon*. Retrieved from <https://es.mathworks.com/help/optim/ug/fmincon.html>
- NASA. (2023a). *Dart: Double asteroid redirection test*. Retrieved from <https://nasa3d.arc.nasa.gov/detail/DART>
- NASA. (2023b). *Mars orbiter mission*. Retrieved from <https://solarsystem.nasa.gov/missions/mars-orbiter-mission/in-depth/>
- Parrish, N. L., & Scheeres, D. J. (2016). Low-thrust trajectory optimization with simplified sqp algorithm.
- R. Bertrand, R. E. (2002). New smoothing techniques for solving bang–bang optimal control problems—numerical results and statistical interpretation.
- Tieding Guo, J. L., Fanghua Jiang. (2011). Homotopic approach and pseudospectral method applied jointly to low thrust trajectory optimization.
- W.Andrew Hoskings, N. J. L. A. T., Randall S.Aadland, & M.Monheiser, J. (2007). Next ion propulsion system production readiness.
- Weber, B. (2023). *Orbital mechanics astrodynamics*. Retrieved from <https://orbital-mechanics.space/intro.html#>
- Wikipedia. (2022). *Coordinate system*. Retrieved from https://en.wikipedia.org/wiki/Coordinate_system
- Wikipedia. (2023a). *Deep space 1*. Retrieved from https://es.wikipedia.org/wiki/Deep_Space_1
- Wikipedia. (2023b). *Double asteroid redirection test*. Retrieved from [https://en.wikipedia.org/wiki/Double_Asteroid_Redirection_Test#:~:text=DART%20demonstrated%20the%20NEXT%20gridded,\(NEXT%2DC\)%20engine](https://en.wikipedia.org/wiki/Double_Asteroid_Redirection_Test#:~:text=DART%20demonstrated%20the%20NEXT%20gridded,(NEXT%2DC)%20engine).
- Wikipedia. (2023c). *Hayabusa*. Retrieved from <https://en.wikipedia.org/wiki/Hayabusa>
- Wikipedia. (2023d). *International celestial reference system and its realizations*. Retrieved from https://en.wikipedia.org/wiki/International_Celestial_Reference_System_and_its_realizations
- Wikipedia. (2023e). *Particle swarm optimization*. Retrieved from https://en.wikipedia.org/wiki/Particle_swarm_optimization
-

Wikipedia. (2023f). *Patched conic approximation*. Retrieved from https://en.wikipedia.org/wiki/Patched_conic_approximation

Wikipedia. (2023g). *Spacecraft electric propulsion*. Retrieved from https://en.wikipedia.org/wiki/Spacecraft_electric_propulsion

Ya-Zhong Luo, H.-y. L., Guo-Jin Tang. (2006). Optimization of multiple-impulse minimum-time rendezvous with impulse constraints using a hybrid genetic algorithm.

Part II

Budget and specifications

Chapter 7

Specifications

7.1 Introduction

In this section, a series of appendices and their sections are explained and detailed, with the aim of making it clear that the current regulations are complied with in relation to the ordinances of safety, hygiene and health at the workplace.

The ordinances come from Royal Decree 486/1997, of April 14. The Law 31/1996, of November 8, represents the legal norm of Occupational Risk Prevention. Specifically, it is article 6 of this law that establishes the technical regulation that guarantees the safety and health of the workplace.

The workplace where the project is carried out is an office located in the CMT - Thermal Motors building. Therefore, it is intended to make it clear that the working conditions met in these two spaces.

7.2 Appendix I: General safety conditions in workplaces

Appendix I represents the applicable regulation to the work area used from the entry into force of the aforementioned Royal Decree.

Section 1 - Structural safety establishes that work platforms, ladders and stairs must have the strength and resistance to support the loads or efforts to which they are subjected. In addition, a reinforced system is needed that ensures stability and, of course, not to overload the elements mentioned above. The work area used meets this requirement.

Section 2 - Work spaces and dangerous areas sets a minimum spacing of the work area in order to ensure safety, health and ergonomic conditions. In addition, it

mentions the need to mark those areas with a risk of falling objects that pose a danger to the worker. The work area used meets this requirement.

Section 3 - Floors, openings and unevenness, and railings leaves it clear that the characteristics of the floors are stable, fixed and non-slip. On the other hand, openings with a risk of falling must have railings with rigid materials and with certain minimum dimensions. The work area used meets this requirement.

Section 4 - Partitions, windows and openings manifests, on the one hand, that the partitions are clearly marked and made with safe materials. In addition, the windows must have a safe opening and closing, with the possibility of cleaning without risk to the worker who performs this action. The work area used meets this requirement.

Section 5 - Circulation routes maintain the design in accordance with a specific use. It is necessary to take into account the potential number of users and, once this is done, to secure stairs, corridors, ramps and loading docks in accordance with their intended use. The work area used meets this requirement.

Sections 6, 7, 8 and 9 - Doors, gates, ramps, fixed and service stairs, fixed ladders and stepladders reveal a number of sizing points. The work area used meets this requirement.

Section 10 - Evacuation routes and exits assumes a series of points in which the opening mode of doors, dimensions, distribution and signaling are mentioned. The work area used meets this requirement.

Section 11 - Fire protection conditions establishes the need to modify the fire fighting devices in relation to the maximum number of people. The work area used meets this requirement.

Section 12 and 13 - Electrical installation and disabled people, finally, assume that, on the one hand, the electrical installation does not pose a risk of fire or explosion, and on the other hand, the work space must be conditioned for disabled workers. The work area used meets this requirement.

7.3 Order, cleaning and maintenance

In the present appendix, it is mainly mentioned that; the circulation areas, exits and circulation routes in the workplaces must be used without any difficulty, the work spaces must be cleaned and maintained with a certain periodicity, the ventilation installation must be kept in good condition, and that the cleaning action must not pose a new risk for workers. The work area used meets this requirement.

7.4 Appendix III: Environmental conditions of workplaces

The environmental conditions, in the first place, must not pose any discomfort or discomfort for the workers. Therefore, in this appendix, an interval of temperature and relative humidity is established that allows for adequate work in a closed workplace. In addition, the need for effective air renewal of the premises is mentioned. In the case of outdoor work, workers must be protected from any inclement weather. The work area used meets this requirement.

7.5 Appendix IV: Lighting of workplaces

The lighting should preferably be natural. Otherwise, the visual requirements of the tasks themselves can be adapted with artificial lighting. In Appendix IV, in addition, establishes a minimum lighting depending on the areas and tasks. In addition to this, some points to be met are fixed, which deal with the distribution and the specific mode of use in each case. The work area used meets this

7.6 Appendix V: Toilet facilities and rest areas

Appendix V mentions the need for drinking water. On the other hand, it deals with the minimum requirements that must exist in changing rooms, showers, and toilets. In addition, the use of rest areas is mentioned whenever the health of workers requires it.

In the case of temporary premises and outdoor work, rest areas are needed, always depending on the demands of workers, as well as dormitories and dining rooms in case the residence is far from the work area. The work area used meets this requirement.

7.7 Appendix VI: First aid materials and facilities

First aid materials are influenced by the number of workers. A portable first-aid kit containing specific materials is necessary, and this material must be distributed in such a way as to ensure a quick response to foreseeable damage. On the other hand, first-aid facilities must have at least a first-aid kit, a stretcher, and a source of drinking water. The work area used meets this requirement.

Chapter 8

Budget

8.1 Introduction

The budget for this project is calculated. For this purpose, the cost of personnel, material - various computer licenses - and services - electricity, transport, etc. - are taken into account. The currency used is the Euro [€], and the time of use is counted in hours [h].

8.2 Cost breakdown

First, the unit cost of the activities is developed depending on their nature.

8.2.1 Material

The section takes into account the cost of workstation hardware, computer licenses, and writing utensils.

Workstation

A MSI WE62 7RI laptop with an Intel Core i7-7700 processor and 16 GB of RAM was purchased for the project.

On the one hand, the amortization cost assumes a 7-year amortization period. The initial cost of the laptop and its current market price are taken into account. On the other hand, the amortized cost corresponds to one academic year -the time of Master Thesis completion-.

Concept	Amount[€]
Initial acquisition cost	2200
Final selling cost	950
Annual depreciation cost	178.57
Total	178.57

Table 8.1: Annual depreciation cost

Computer licenses

The computer licenses take into account all the costs involved in the use of calculation, editing, and presentation programs for the project. The programs and the hourly cost of their use are shown in the table 8.2. The total represented is calculated with the following hourly computation:

- 250 MATLAB hours
- 40 Microsoft Office hours

Concept	Amount [€]
MATLAB cost per hour	0.03
\LaTeX cost per hour	0
Microsoft Office cost per hour	0.01
Total	7.9

Table 8.2: Computer license total cost

Cost of writing materials

It is necessary to count the cost of printed material, in addition to writing utensils such as pens, etc. Table 8.3 shows the final value of these materials.

Concept	Amount [€]
Writing materials	5
Total	15

Table 8.3: Cost of writing materials

8.2.2 Personnel hours

On the one hand, the hourly salary of a full professor of the university -project tutor- is considered. On the other hand, the cost per hour earned by a student on an internship in the IMM department is taken into account. The hours used in the work are:

- 400 author hours
- 30 tutor 1 hours
- 30 tutor 2 hours

Concept	Amount [€]
Tutor cost per hour	20
Author cost per hour	5
Total	3200

Table 8.4: Personnel hours cost

8.2.3 Electricity consumption

Electricity consumption is the last of the expenses to be taken into account. The calculation of transportation for commuting is not considered, since neither public nor private transportation has been used. In the table 8.5 the 5.113 % electricity tax has been accumulated. Electricity consumption varies approximately around 0.15 €/kWh, this being the value considered.

Concept	[W]	[kWh]	Amount [€]
Laptop	120	48	7.57
Air conditioner	1000	100	15.77
Light	400	32	5.05
Total			28.39

Table 8.5: Electricity consumption

8.3 Final cost

To the sum of the above numbers, it should be considered the VAT percentage of 21%. Hence, the final value can be seen in Table 8.6.

Concept	Amount [€]
Material	201.47
Personnel hours	3200
Electricity consumption	28.39
Total + VAT	3429.86

Table 8.6: Final cost

The budget is

**THREE THOUSAND FOUR HUNDERD TWENTY-NINE EUROS
AND EIGHTY-SIX CENTS**

8.4 Commercial profit

The previously calculated cost must be compensated with the possible commercial benefit obtained from the study carried out. In real life, a market study must be carried out and the business strategy must be planned so that finally the commercial benefit is roughly estimated.

However, an approximation of between 4% to 10% commercial net profit to revenue can be assumed, as stipulated by the private firm Deloitte Touche Tohmatsu Limited in the 2018 financial study on the aerospace and defense industry

Assuming the final degree work is performed by a start-up company, a loss of 15% should be added with respect to net income for corporate income tax purposes.

Therefore, in the worst case, the business profit is 137.19 € and in the best case a 342.98 €. On these profits, a corporate income tax of 20.58 € and 51.44 € respectively is obtained.

Therefore, with the new cost added by the corporate income tax,

The minimum commercial benefit is

ONE HUNDRED SIXTEEN EUROS AND SIXTY-ONE CENTS

The maximum commercial benefit is

TWO HUNDERD NINETY-ONE EUROS AND FIFTY-FOUR CENTS